J Adv Ceram

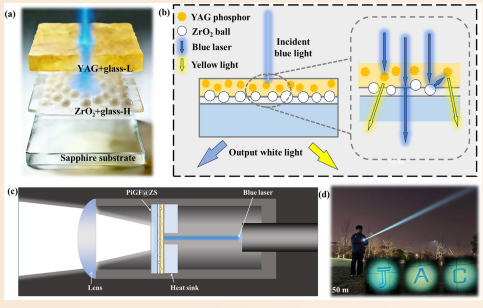
Research Article

A novel PiGF@ZS color converter with a ZrO_2 microsphere-embedded reflector for high-brightness laser lighting

Hongjin Zhang, Wei Cheng, Tao Lu, Jiuzhou Zhao, Xiaowei Liu, Yang Peng✉

Cite this article: Zhang HJ, Cheng W, Lu T, et al. *J Adv Ceram* 2026, **15**(7): 9221327. https://doi.org/10.26599/JAC.2026.9221327

ABSTRACT: Luminescence saturation of static color converters represents a pivotal hurdle for the progression of next-generation high-brightness laser lighting. The conventional phosphor-in-glass film (PiGF) color converter faces inherent limitations in achieving high luminous efficacy (LE), constrained by insufficient phosphor excitation under focused laser irradiation and optical losses at the film-substrate boundary. Herein, a novel PiGF@sapphire (PiGF@S) converter with a ZrO_2 microsphere-embedded reflector (PiGF@ZS) was proposed for laser lighting. This designed microstructure effectively reflects unabsorbed blue light back to the phosphor layer, significantly enhancing light utilization efficiency and LE for high-power laser lighting. Furthermore, the effects of laser spot diameters on the luminescence saturation were investigated in the PiGF@ZS converter. Benefiting from this synergistic opto-thermal design, the optimized PiGF@ZS converter exhibits a high LE of 240.5 lm/W and a maximum luminous flux (LF) of 3782 lm at a 25 W laser (5 mm spot). Notably, under a 3 W laser with a spot diameter of 1 mm, the PiGF@ZS converter achieves an LF 1.2 times that of a conventional PiGF@S converter. Owing to the enlarged excitation area and improved heat dissipation, the PiGF@ZS converter achieves a lower surface temperature of 54.6 °C under a 3 W laser with a 5 mm spot compared with 61 °C for the PiGF@S converter, demonstrating enhanced thermal management capability. The microstructured ZrO_2 interface effectively mitigates thermal accumulation and enhances blue light utilization efficiency for PiGF-based laser lighting.



KEYWORDS: laser lighting; laser spot diameter; luminous efficacy; color converters; phosphor-in-glass film

1 Introduction

Compared with traditional light-emitting diode (LED) sources, laser diodes (LDs) deliver superior spatial coherence and spectral purity while eliminating the efficiency droop issue [1–5], thereby offering a compelling pathway toward next-generation high-brightness collimated lighting [6–10]. Accordingly, blue laser-driven color converters have emerged as the cornerstone of modern high-brightness lighting architectures [11–15]. However, the intrinsically small spot size of blue laser beams subjects converters to extreme irradiance and intense thermal loading, necessitating exceptional optical stability and thermal management capabilities [16–20]. In response to these stringent requirements, a variety of all-inorganic converters have been developed, including single crystals (SCs) [21–23], phosphor ceramics (PCs) [24–26], phosphor-in-glasses (PiGs) [27], and phosphor-in-glass films (PiGFs) [28–31]. PiGF has garnered particular attention due to its thin-film architecture, facile preparation, low cost, and excellent compatibility with substrate materials, making it a promising candidate for high-power laser lighting applications [32–36].

In a typical white laser diode (W-LD) system, a blue laser excites a color converter to generate yellow light via photoluminescence, with the remaining blue light mixing to produce white emission [37–41]. However, the highly collimated and tightly focused nature of the laser beam confines the excitation to a small area, engaging fewer phosphor particles. This problem leads to inefficient blue–yellow conversion and nonuniform color distribution [42–47]. Recently, Wang *et al.* [48] developed a PiGF@sapphire converter with Ta_2O_5/SiO_2 multilayer coatings, achieving dual optical functions (anti-reflection (AR) coating for blue light, high-reflection (HR) coating for visible light) and a luminous efficacy (LE) of 213.7 lm/W@12.9 W/mm^2. While effective in enhancing forward emission, this coating-based approach primarily addresses the light propagation direction rather than recycling unabsorbed blue light that scatters within the phosphor layer. Moreover, the multilayer structure may introduce additional interfacial thermal resistance under high-power operation. Recognizing the critical need for LE enhancement in transmissive color converters, our group has conducted systematic research in this area, including sandwiched bilayer structures for photon reabsorption management [49,50], reflective cup designs for backward light collection [51], and microstructured substrates for blue light recycling [52]. Peng *et al.* [49] developed a sandwiched green–red PiGF structure on double sides of sapphire (G-S-R PiG), which effectively couples photon reabsorption and

School of Aerospace Engineering, Huazhong University of Science and Technology, Wuhan 430074, China.

✉ Corresponding author. E-mail: ypeng@hust.edu.cn

Received: March 23, 2026; Revised: April 28, 2026; Accepted: May 23, 2026

© The Author(s) 2026. This is an open access article under the terms of the Creative Commons Attribution 4.0 International License (CC BY 4.0, http://creativecommons.org/licenses/by/4.0/).

backward scattering, yielding a high LE of 163 lm/W and an excellent color rendering index (CRI) of 85.4 at a laser power of 2.4 W. Yu *et al.* [50] developed a universal PiGF@sapphire@MiG converter with a MgO-in-glass layer coated on the opposite side of sapphire, which recycles backscattering light and improves heat dissipation, achieving a high luminous flux (LF) of 5515 lm and an LE of 196.9 lm/W at a saturation threshold of 28 W/mm^2. Mou *et al.* [51] proposed a reflective PiGF converter with a mirror Al reflection cup to collect backward emission light and enhance heat dissipation, achieving a saturation threshold of 15 W/mm^2 and a maximum LF of 1925.3 lm, which are over twice as high as those of the traditional transmissive PiGF converter. Currently, considerable attention has been devoted to the microstructuring of heat-conducting substrates to enhance the optical performance of phosphor converters. To mitigate such interfacial scattering losses, a recent approach by Zhao *et al.* [52] employed a moth-eye microstructure on a sapphire substrate (PiGF–MS), demonstrating an 11% improvement in LE at 2.39 W laser excitation over conventional PiGF. Similarly, Ding *et al.* [53] developed a high-performance PiGF on a patterned sapphire substrate (PSS–PiF). The periodic conical structures on PSS not only increase the contact area between the PiF and substrate by approximately 56%, forming a more robust film composite but also induce a diffraction effect that disperses the convergent laser beam, significantly expanding the spot area and improving light uniformity. Consequently, the PSS–PiF converter achieved a saturation power density of 6.29 W/mm^2 (91% higher than that on flat sapphire substrates) while maintaining a high luminous efficacy of 220 lm/W. Despite this performance enhancement, the complexity and cost associated with microstructuring sapphire substrates restrict its viability for mass production and widespread use in the PiGF converter.

Herein, we conceived a novel PiGF@sapphire (PiGF@S) color converter with a ZrO_2 microsphere-embedded reflector (PiGF@ZS) for laser lighting. In the fabrication process of PiGF@ZS, the PiGF and ZrO_2-in-glass (ZiG) layers are sintered using glass powders with different glass transition temperatures (high-T_g glass powder for the ZiG layer and low-T_g glass powder for the PiGF layer). This design ensures the structural integrity of the ZiG layer during sintering, while the relatively lower sintering temperature preserves the quantum efficiency of $Y_3Al_5O_{12}:Ce^{3+}$ (YAG) phosphor particles by minimizing thermal degradation. In this architecture, the incident blue laser is reflected by the microstructured ZiG interface, which significantly enhances the absorption probability of blue photons by the overlying YAG phosphor layer and improves the conversion efficiency of yellow light. As a result, the laser-driven PiGF@ZS converter exhibits an exceptional LE of 240.5 lm/W and achieves a maximum LF of 3782 lm under 25 W laser excitation (5 mm spot diameter). Notably, at a small spot diameter of 1 mm under 3 W excitation, the PiGF@ZS converter delivers an LF 1.2 times as high as that of conventional PiGF@S. Such a dramatic improvement underscores the effectiveness of the proposed microstructure interface in overcoming the fundamental limitations of PiGF, including severe thermal accumulation and insufficient blue light utilization. Finally, an outdoor irradiation test was conducted to validate the practical feasibility of the PiGF@ZS-based laser lighting system.

2 Experiments

2.1 Materials

Commercially procured $Y_3Al_5O_{12}:Ce^{3+}$ (YAG) phosphor from Intematix Co. was used as the precursor material. High-T_g glass powder (B_2O_3–SiO_2–ZnO–Li_2O–La_2O_3–WO_3, T_g = 368 °C) was purchased from SCHOTT AG, Germany. Low-T_g glass powder (B_2O_3–SiO_2–Na_2O–P_2O_5–Al_2O_3, T_g = 225 °C) was synthesized via the conventional melt-quenching method. The organic solvent was formulated by mixing ethyl cellulose (Sinopharm, China) with terpineol (Aladdin, China) under stirring at 80 °C for 20 min. A sapphire plate measuring 15 mm × 15 mm × 1 mm was employed as the thermally conductive substrate. ZrO_2 microspheres with diameters of 100–120 μm were commercially obtained.

2.2 Fabrication of the PiGF@ZS converter

Figure 1 illustrates the fabrication process of the PiGF@ZS converter. First, the phosphor-glass paste was prepared by mixing YAG phosphor particles, low-T_g glass powder, and organic solvent, with a phosphor-to-glass mass ratio of 40 wt%. Separately, the ZrO_2-glass pastes were formulated by blending ZrO_2 microspheres, high-T_g glass powder, and organic solvent at a ZrO_2-to-glass mass ratio of 1 : 2. After that, the ZrO_2-glass pastes were uniformly coated onto the sapphire substrates and then dried at 110 °C for 30 min, yielding a ZiG layer thickness of 100 μm. The samples were subsequently held at 550 °C for 1 h. During the sintering process, the glass layer densified, resulting in a thickness reduction to 50 μm. Consequently, the larger ZrO_2 microspheres (100–120 μm) protruded from the surface, forming a simply microstructured substrate. Subsequently, the YAG-glass paste was coated onto the ZiG layer and dried at 110 °C for 30 min. The samples were then sintered at 350 °C for 1 h. Since this sintering temperature is lower than the glass transition temperature of the high-T_g glass powder used in the ZiG layer, the structural integrity of the underlying ZiG layer was well preserved. Meanwhile, the relatively low sintering temperature also minimized thermal degradation of the YAG phosphor, ensuring its quantum efficiency.

2.3 Characterizations

The morphology and elemental mapping of the PiGF@ZS converter were examined using a scanning electron microscope (SEM; GeminiSEM 350, Carl Zeiss, Germany) equipped with an energy-dispersive X-ray spectrometer (EDS; D9 ADVANCE, UK). The crystalline phases were identified by an X-ray diffractometer (XRD; Empyrean, PANalytical B.V., the Netherlands). The optical properties, including photoluminescence (PL) and photoluminescence excitation (PLE) spectra, decay curves, and quantum yield, were measured using a fluorescence spectrometer (QuantaMaster 8500, Horiba Instruments, Canada). The optical performance of PiGF converters under different laser powers was evaluated using a custom-built system equipped with a 450 nm blue LD (50 W), an integrating sphere (50 cm), and a spectrometer (HAAS-2000, EVERFINE, China). The parameters of EL spectra, LF, LE, and correlated color temperature (CCT) were obtained. Simultaneously, the surface temperatures of the PiGF converters were captured by an infrared thermal camera (FLIR E63, USA).

3 Results and discussion

The cross-sectional SEM images of the PiGF@ZS converter reveal a well-defined bilayer structure with no visible voids or delamination, as shown in Fig. 2. The upper PiGF layer (100 μm) and the lower ZiG layer (50 μm) are tightly bonded to each other, both exhibiting excellent adhesion to the sapphire substrate without cracks or interfacial debonding. Within the PiGF layer, the YAG phosphor particles are uniformly embedded in the low-T_g glass matrix, with clear boundaries between the phosphor and

glass phases. The EDS elemental mapping confirms the presence and distribution of Y, Al, Si, and Zr throughout the converter. In the PiGF layer (Fig. 2(a)), the Al element is distributed throughout both the YAG phosphor particles and the surrounding low-T_g glass matrix. In the underlying ZiG layer (Fig. 2(b)), the Si signals are exclusively observed, corresponding to the high-T_g glass matrix, and the Zr signals are localized around the embedded ZrO_2 microspheres. The PiGF surface (Fig. 2(c)) shows evenly distributed phosphor particles with no visible porosity. The surface morphology of ZiG (Fig. 2(d)) displays uniformly dispersed ZrO_2 microspheres embedded in a dense glass matrix. These results confirm that the structural integrity and elemental distribution of both glass layers and phosphor particles are well preserved during the sintering process, with no detectable interdiffusion or degradation.

The PL and PLE spectra of the YAG phosphor and PiGF converter are shown in Fig. 3(a). The characteristic Ce^{3+} 4f → 5d transition gives rise to an excitation peak at approximately 470 nm in the YAG phosphor. When irradiated by a 450 nm blue laser, the PiGF converter emits broadband yellow light with a peak wavelength of approximately 540 nm. The XRD patterns in Fig. 3(b) reveal that PiGF retains all characteristic diffraction peaks

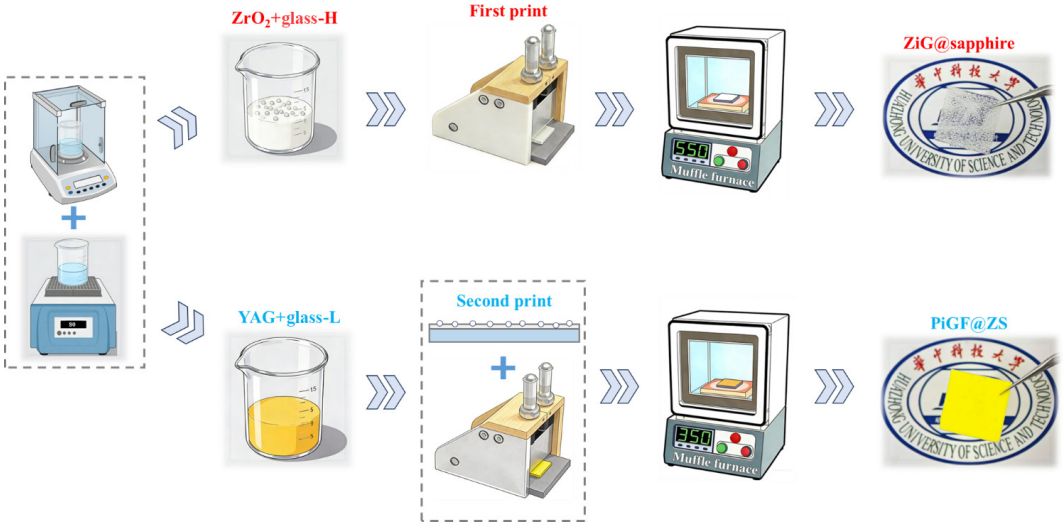


Fig. 1 Schematic illustration of fabrication process of PiGF@ZS converters.

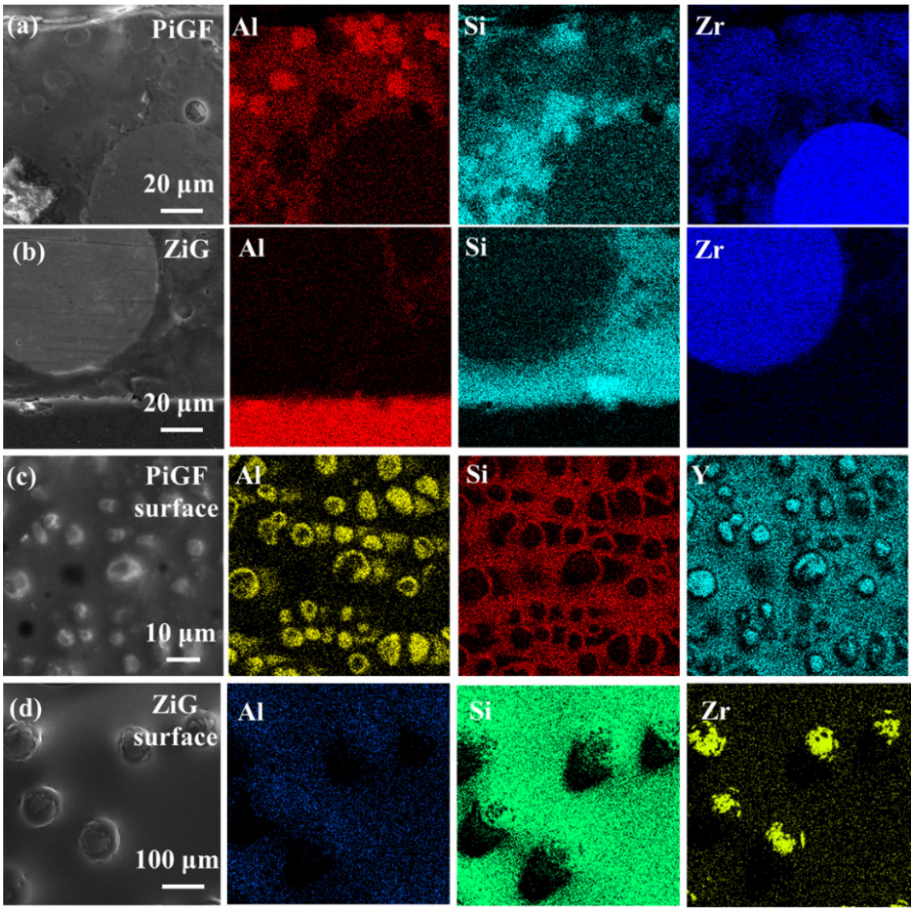


Fig. 2 SEM images and EDS mapping images of (a) cross-sectional PiGF, (b) cross-sectional ZiG, (c) PiGF surface, and (d) ZiG surface.

清華大学出版社 Tsinghua University Press | SciOpen

of the YAG phosphor without any shift or additional phases across the 2θ range of 10°–80°, further evidencing the preservation of phosphor crystallinity after sintering. The decay lifetimes (Fig. 3(c)) between the raw phosphor and the PiGF confirm that the luminescence mechanism of the YAG phosphor remains unaffected by the fabrication process. The thermal properties of the glass powders were characterized by differential scanning calorimetry–thermogravimetry (DSC–TG) (Figs. 3(d) and 3(e)). The low-T_g glass exhibits a glass transition at 225 °C, while the high-T_g glass shows a T_g of 368 °C. The selection of 350 °C as the sintering temperature for PiGF is strategically chosen because it is sufficiently above the low-T_g glass to enable densification but below the high-T_g glass to maintain the ZiG and prevent collapse of ZrO_2 microspheres. Figure 3(f) demonstrates that the PiGF@ZS converter retains a high internal quantum efficiency (QE) of 82.1%, compared with 85.9% for the YAG phosphor. The minimal 3.8% degradation confirms the effectiveness of the material selection and thermal management strategy. By employing low-T_g glass (T_g = 225 °C) for PiGF, sintering at 350 °C is sufficient for glass densification yet mild enough to preserve the phosphor crystal structure. Meanwhile, the underlying ZiG, sintered at 550 °C using high-T_g glass (T_g = 368 °C), remains unaffected during the second sintering step.

The light propagation mechanism within the laser-driven PiGF@ZS converter is schematically depicted in Figs. 4(a)–4(c). In this architecture, the incident blue laser is reflected by the microstructured ZiG interface, which significantly enhances the absorption probability of blue photons by the overlying YAG phosphor layer and thus improves the conversion efficiency of yellow light. Unlike conventional PiGF converters, where a substantial portion of blue light is transmitted through the phosphor layer without interaction, the protruding ZrO_2 microspheres in our design redirect unabsorbed blue photons back into the PiGF layer. This light recycling effect extends the optical path length of blue photons within the phosphor layer, enabling multiple scattering events and increasing the likelihood of absorption by phosphor particles. Figure 4(d) presents the EL spectra of PiGF@ZS measured at a laser power of 3 W with varying spot diameters. The yellow emission intensity increases progressively as the spot diameter expands from 1 to 5 mm, revealing a distinct positive correlation between the excitation area and radiative output. This enhancement is attributed to a larger spot diameter activating a greater number of phosphor particles for light conversion while simultaneously providing an expanded heat dissipation region that mitigates localized thermal accumulation. Consequently, both the saturation threshold and LE increase with larger spot diameters. Benefiting from this effect, the optimized PiGF@ZS converter delivers a maximum LF of 3782 lm@25 W (Fig. 4(e)) with a 5 mm spot diameter, demonstrating excellent resistance to luminescence saturation under high-power excitation. In contrast, the conventional PiGF@S converter saturates at a lower laser power of 22 W with a reduced LF of 3327 lm under the same spot diameter (Fig. 4(f)). Notably, at a small spot diameter of 1 mm under 3 W excitation, the PiGF@ZS converter delivers an LF 1.2 times as high as that of the conventional PiGF@S. Moreover, the PiGF@ZS converter demonstrates an impressive LE of 240.5 lm/W under 3 W laser excitation with a 5 mm spot diameter. This high LE results from the synergistic effect of enhanced blue light recycling by the ZrO_2-microsphere interface and efficient heat dissipation through the sapphire substrate, which together maximize light output while minimizing thermal losses (Fig. 4(g)). Notably, under 3 W laser excitation, the CCT of PiGF@ZS remains consistently lower than that of PiGF@S across all spot diameters. This indicates a warmer white emission, which can be attributed to the enhanced blue light recycling by the ZrO_2-microsphere interface: The additional absorption of blue photons increases the yellow-to-blue ratio in the output spectrum, shifting the overall white balance toward lower CCT values (Fig. 4(h)). These results confirm that the microstructured ZrO_2 interface effectively recycles unabsorbed blue light and benefits thermal management, positioning the PiGF@ZS converter as a promising candidate for high-brightness laser lighting applications.

Given the critical role of thermal management in high-power laser lighting, the operating temperatures of the PiGF@ZS converter with different laser spot diameters were systematically evaluated under various laser powers and compared with the conventional PiGF@S converter, as presented in Fig. 5(a). The

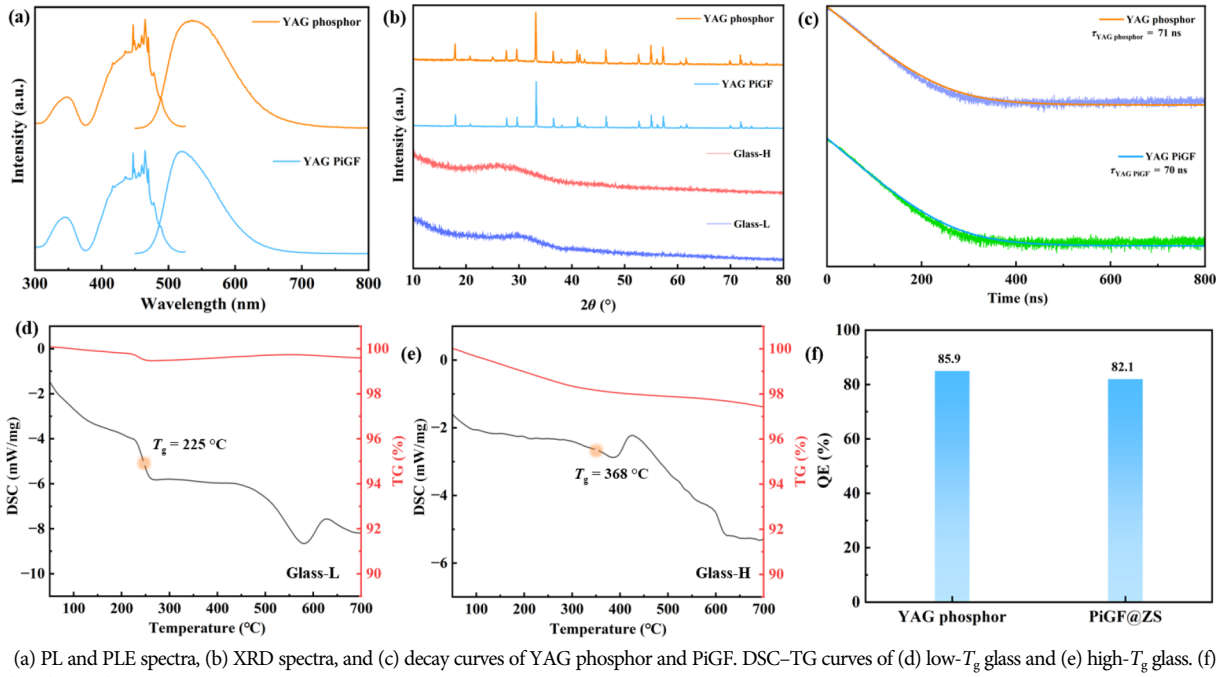


Fig. 3 (a) PL and PLE spectra, (b) XRD spectra, and (c) decay curves of YAG phosphor and PiGF. DSC–TG curves of (d) low-T_g glass and (e) high-T_g glass. (f) QE of YAG phosphor and PiGF@ZS.

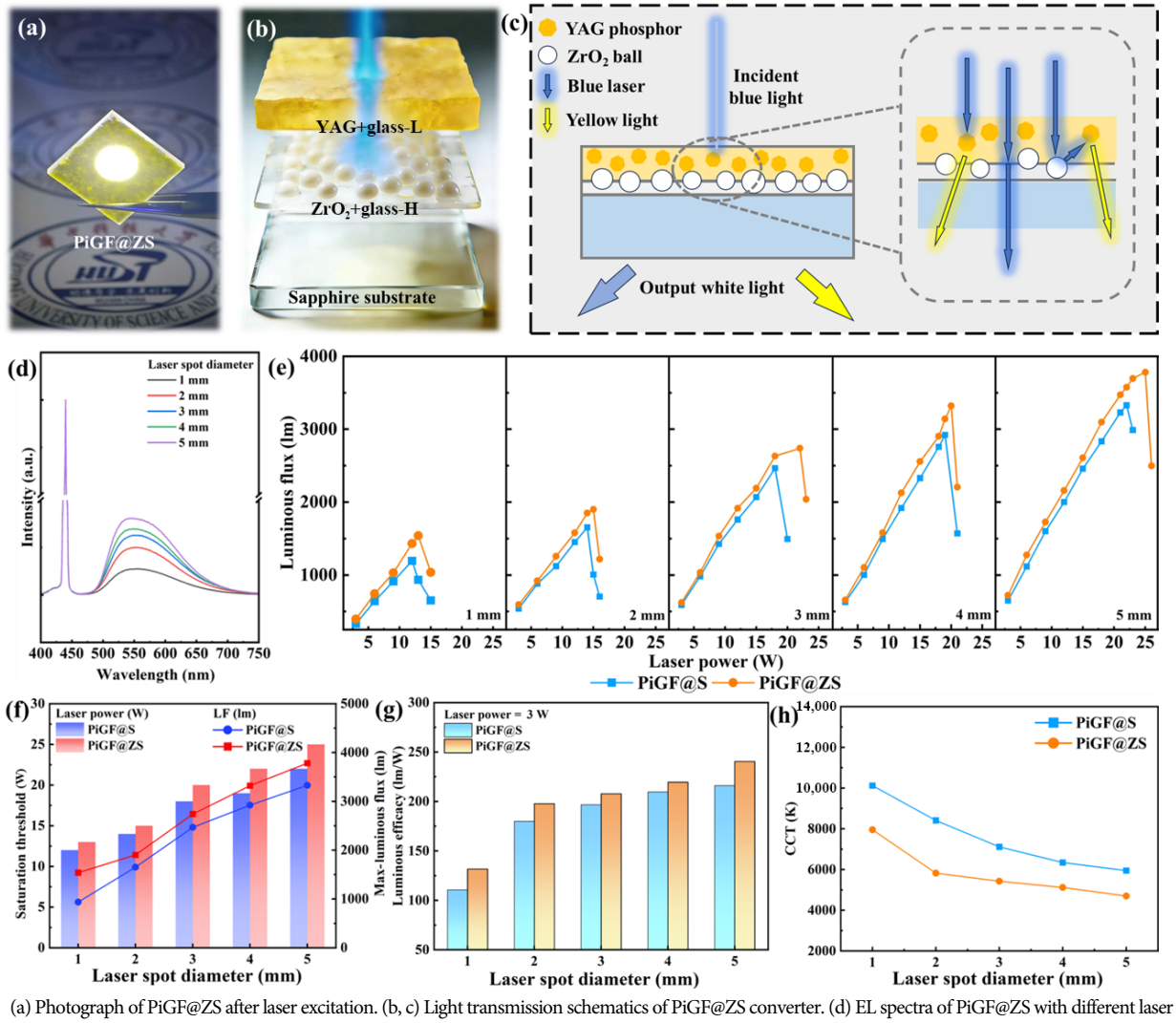


Fig. 4 (a) Photograph of PiGF@ZS after laser excitation. (b, c) Light transmission schematics of PiGF@ZS converter. (d) EL spectra of PiGF@ZS with different laser spot diameters at a laser power of 3 W. (e) LF of PiGF@ZS converter with different laser spot diameters. (f) Saturation threshold and maximum LF of PiGF@ZS and PiGF@S with different laser spot diameters. (g) LE and (h) CCT of PiGF@ZS and PiGF@S with different laser spot diameters at a laser power of 3 W.

improved thermal performance of PiGF@ZS can be attributed to the enhanced blue light recycling by the ZrO_2 microsphere-embedded interface. By reflecting unabsorbed blue photons back into the phosphor layer for additional conversion, fewer photons are transmitted through the converter and converted into waste heat, effectively reducing the thermal load on the phosphor layer. Additionally, the thin-film architecture and direct contact with the high-thermal-conductivity sapphire substrate facilitate efficient heat dissipation, further suppressing the temperature rise under high-power excitation. The dependence of the maximum operating temperature on the laser power was investigated for PiGF@ZS converters after 10 s with varying spot diameters, as illustrated in Fig. 5(b). For all tested spot diameters, upon increasing the laser power from 3 W to the saturation threshold, the maximum operating temperature of PiGF converters undergoes a steep nonlinear escalation. Notably, at a given laser power, the operating temperature decreases significantly as the spot diameter expands from 1 to 5 mm. This trend can be attributed to the enlarged excitation area, which distributes the thermal load over a broader region and reduces localized heat accumulation, thereby suppressing the overall temperature rise. Figure 5(c) further compares the maximum operating temperatures of PiGF@ZS and PiGF@S under 3 W excitation with different spot diameters after 10 s, revealing that PiGF@ZS maintains consistently lower temperatures across all spot sizes. As the laser spot diameter expands from 1 to 5 mm, the maximum surface temperature of PiGF@S drops from 149 to 61 °C, whereas that of PiGF@ZS declines from 106 to 54.6 °C. The corresponding light and heat powers of both converters under 3 W excitation were quantitatively analyzed, as presented in Fig. 5(d). For both converters, the light output power increases progressively with increasing spot diameter, while the heat generation decreases accordingly. Notably, the PiGF@ZS converter exhibits higher light power than PiGF@S across all spot diameters, confirming its superior conversion efficiency enabled by the microstructured ZrO_2 interface. The temperature evolution of PiGF@ZS under 3 W excitation with different spot diameters over 60 s is presented in Fig. 5(e). For spot diameters of 0.5 and 1.0 mm, the temperature exceeds 600 °C within 40 s, reaching the detection limit of the infrared camera. Other configurations remained measurable throughout the full 60 s, with the 5 mm spot exhibiting the lowest temperature of 489 °C, confirming that a larger excitation area reduces thermal accumulation. A direct comparison at 30 s (Fig. 5(f)) reveals that PiGF@ZS maintains lower temperatures than PiGF@S for all spot diameters, further validating the enhanced heat dissipation enabled by the ZrO_2 microsphere-embedded interface.

To demonstrate its viability for high-brightness lighting, the PiGF@ZS converter was assembled into a white laser diode module [54], as depicted in Fig. 6(a). Upon striking the converter,

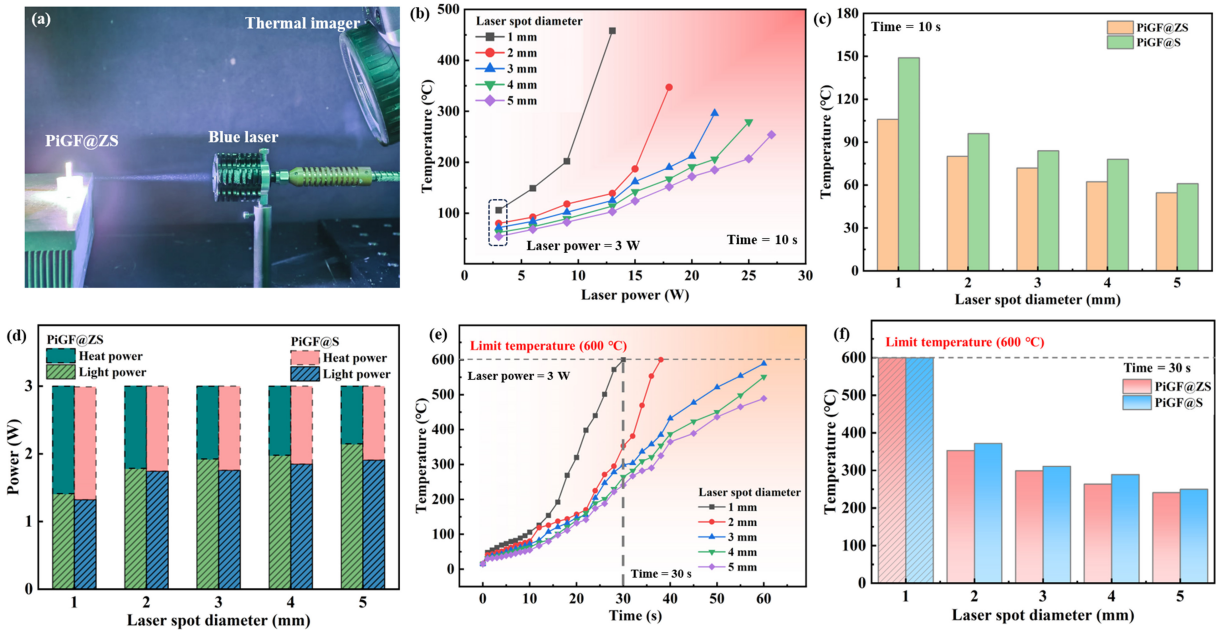


Fig. 5 (a) Surface temperature monitoring system. (b) Maximum operating temperature of PiGF@ZS as a function of laser power for different spot diameters after 10 s. (c) Maximum temperature and (d) light/heat power of PiGF@ZS and PiGF@S under 3 W excitation with different spot diameters. Thermal performance under 3 W excitation with different spot diameters: (e) temperature evolution of PiGF@ZS over 60 s, (f) maximum temperatures of PiGF@ZS and PiGF@S after 30 s.

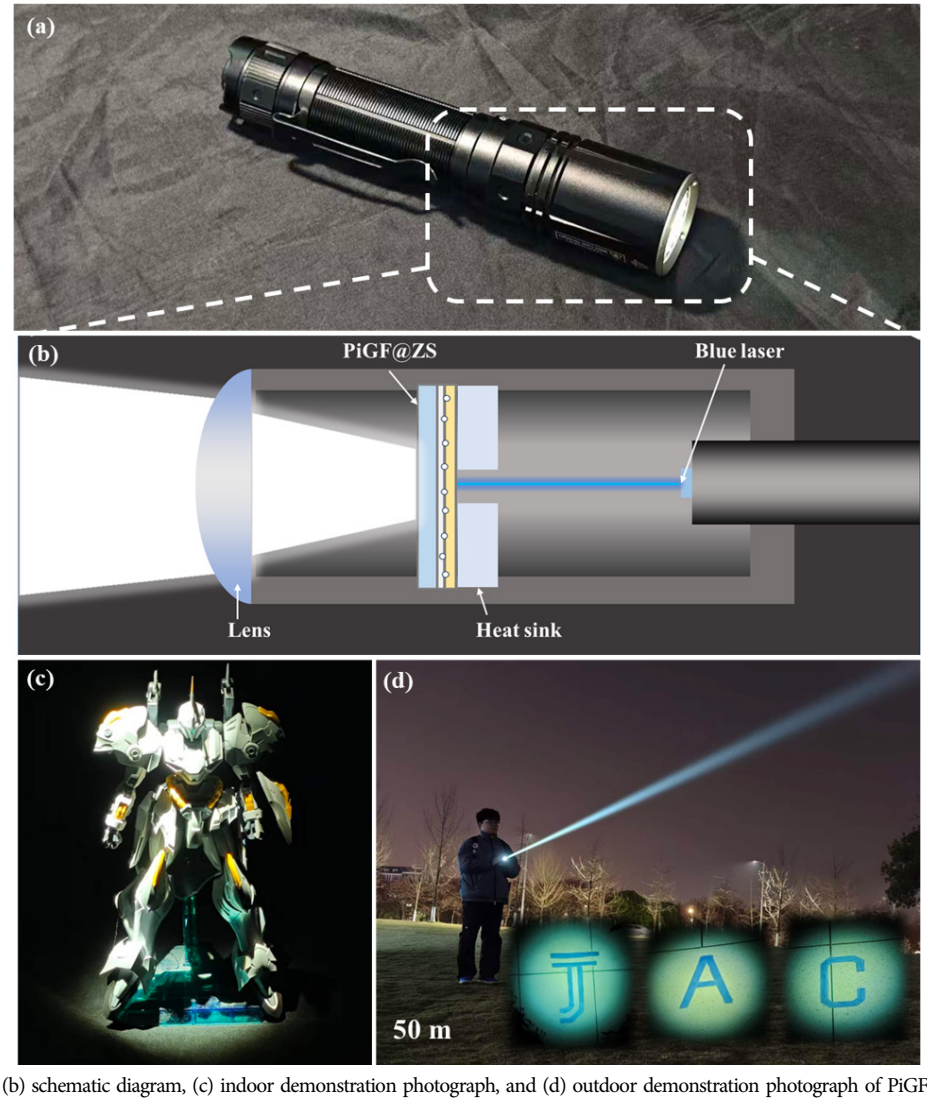


Fig. 6 (a) Photograph, (b) schematic diagram, (c) indoor demonstration photograph, and (d) outdoor demonstration photograph of PiGF@ZS-based laser lighting module.

the incident blue laser is partially absorbed by YAG phosphor particles to produce yellow light, while the unabsorbed portion is reflected by the microstructured ZrO_2 interface back into the phosphor layer for additional conversion. The mixed blue and yellow light then passes through the lens set, resulting in a collimated white beam (Fig. 6(b)). To further evaluate its practical applicability, the assembled laser lighting device was subjected to performance tests in both indoor and outdoor environments, as shown in Figs. 6(c) and 6(d). After transmission exceeds 50 m, the light spot exhibits negligible divergence and accurate color reproduction, underscoring the excellent beam collimation achieved with the PiGF@ZS converter. These characteristics collectively highlight its potential as a superior white laser source for high-brightness field lighting scenarios.

4 Conclusions

In this work, a PiGF@ZS converter with a ZrO_2 microsphere-embedded reflector was proposed for laser lighting. The PiGF@ZS converter was fabricated via a two-step blade-coating process using high-T_g glass for the ZrO_2 microsphere layer and low-T_g glass for the YAG phosphor layer, enabling the formation of a microstructure reflector while preserving the phosphor efficiency. In the PiGF@ZS converter, the embedded ZrO_2 microspheres at the interface function as built-in reflectors, recycling unabsorbed blue photons and extending their optical path within the phosphor layer. This light-trapping effect increases the probability of blue light absorption by YAG phosphor particles, leading to enhanced yellow emission and superior white light output. As a result, the optimized PiGF@ZS converter exhibits a high LE of 240.5 lm/W and a maximum LF of 3782 lm at 25 W (5 mm spot). By redirecting unabsorbed blue photons back into the phosphor layer, it minimizes waste heat generation, enabling the PiGF@ZS converter to maintain a lower operating temperature of 54.6 °C under 3 W excitation with a 5 mm spot diameter, compared with 61 °C for the conventional PiGF@S. Notably, at a small spot diameter of 1 mm under 3 W excitation, it achieves an LF 1.2 times that of conventional PiGF@S, highlighting its great promise for high-power laser lighting.

Acknowledgements

This work was supported by the National Natural Science Foundation of China (No. 52475594), the Hubei Provincial Natural Science Foundation of China (No. 2026AFC0612), the Key Research and Development Program of Wuhan (No. 2025050102030007), and the Natural Science Foundation of Wuhan (No. 2026040101030010). The authors would like to thank the Analytical and Testing Center of Huazhong University of Science and Technology for support with the PL, SEM, decay, and DSC measurements.

Availability of data and materials

The data that support the findings of this study are available from the corresponding author upon reasonable request.

Competing interests

The authors have no competing interests to declare that are relevant to the content of this article.

References

[1] Schubert EF, Kim JK. Solid-state light sources getting smart. *Science* 2005, **308**: 1274–1278.

[2] Sun YS, Wang YZ, Chen WB, *et al.* Rapid synthesis of phosphor-glass composites in seconds based on particle self-stabilization. *Nat Commun* 2024, **15**: 1033.

[3] Liu GC, Chen WB, Xiong Z, *et al.* Laser-driven broadband near-infrared light source with watt-level output. *Nat Photonics* 2024, **18**: 562–568.

[4] Zhang D, Xiao WG, Liu C, *et al.* Highly efficient phosphor-glass composites by pressureless sintering. *Nat Commun* 2020, **11**: 2805.

[5] Sang PF, Zhang L, Kang J, *et al.* Composite structure Al_2O_3/Al_2O_3–YAG:Ce/YAG ceramics with high color spatial uniformity for white laser lighting. *J Adv Ceram* 2024, **13**: 189–197.

[6] Yao Q, Hu P, Sun P, *et al.* YAG:Ce^{3+} transparent ceramic phosphors brighten the next-generation laser-driven lighting. *Adv Mater* 2020, **32**: 1907888.

[7] Cheng ZQ, Liu X, Chen XR, *et al.* Composition and luminescence properties of highly robust green-emitting LuAG:Ce/Al_2O_3 composite phosphor ceramics for high-power solid-state lighting. *J Adv Ceram* 2023, **12**: 625–633.

[8] Zhang YF, Li L, Zhang XS, *et al.* Temperature effects on photoluminescence of YAG:Ce^{3+} phosphor and performance in white light-emitting diodes. *J Rare Earth* 2008, **26**: 446–449.

[9] Liu XC, Yang CC, Li YB, *et al.* High recorded color rendering performance of single-structured Ce,Mn:$Y_3(Al,Sc)_2Al_3O_{12}$ phosphor ceramics for high-power white LEDs/LDs. *J Adv Ceram* 2024, **13**: 810–820.

[10] Huang P, Zhou BY, Zheng Q, *et al.* Nano wave plates structuring and index matching in transparent hydroxyapatite-YAG:Ce composite ceramics for high luminous efficiency white light-emitting diodes. *Adv Mater* 2020, **32**: 1905951.

[11] Zhu SY, Jin SL, Zhan LK, *et al.* Glass network engineering of yellow-emitting $Ba_2Sc_2B_4O_{11}$:Ce^{3+} glass ceramics for full-spectrum lighting. *J Adv Ceram* 2025, **14**: 9221169.

[12] Huang QG, Lin H, Wang B, *et al.* Patterned glass ceramic design for high-brightness high-color-quality laser-driven lightings. *J Adv Ceram* 2022, **11**: 862–873.

[13] Shen WC, Azmy A, Li G, *et al.* A crystalline 2D fullerene-based metal halide semiconductor for efficient and stable ideal-bandgap perovskite solar cells. *Adv Energy Mater* 2024, **14**: 2400582.

[14] Tang QH, Yuan X, Zou M, *et al.* Mismatched refractive index strategy for fabricating laser-driven wood diffusers from bulk wood for illumination applications. *Adv Mater* 2024, **36**: 2306593.

[15] Zhao JT, Lei L, Ye RG, *et al.* Sunlight activated ultra-stable long persistent luminescence glass ceramic for outdoor information display. *J Adv Ceram* 2022, **11**: 974–983.

[16] Yang ZZ, Zheng S, Xi GY, *et al.* Patterned phosphor-in-glass films with efficient thermal management for high-power laser projection displays. *J Adv Ceram* 2023, **12**: 2075–2086.

[17] Xi GY, Lin SS, Shen TJ, *et al.* Transparent ceramic@sapphire composites for high-power laser-driven lighting. *Adv Sci* 2025, **12**: 2505232.

[18] Zhang R, Lin H, Yu YL, *et al.* A new-generation color converter for high-power white LED: Transparent Ce^{3+}:YAG phosphor-in-glass. *Laser Photonics Rev* 2014, **8**: 158–164.

[19] Zhang XJ, Si SC, Yu JB, *et al.* Improving the luminous efficacy and resistance to blue laser irradiation of phosphor-in-glass based solid state laser lighting through employing dual-functional sapphire plate. *J Mater Chem C* 2019, **7**: 354–361.

[20] Yu ZK, Zhao JZ, Wang Q, *et al.* Laser spot associated high-saturation phosphor-in-glass film for transmissive and reflective high-brightness laser lighting. *J Adv Ceram* 2023, **12**: 1821–1832.

[21] Zheng P, Li SX, Takeda T, *et al.* Unraveling the luminescence quenching of phosphors under high-power-density excitation. *Acta Mater* 2021, **209**: 116813.

[22] Cantore M, Pfaff N, Farrell RM, *et al.* High luminous flux from single crystal phosphor-converted laser-based white lighting system. *Opt Express* 2016, **24**: A215–A221.

[23] Park KW, Lim SG, Deressa G, *et al.* High power and temperature luminescence of $Y_3Al_5O_{12}$:Ce^{3+} bulky and pulverized single crystal phosphors by a floating-zone method. *J Lumin* 2015, **168**: 334–338.

[24] Qiang YC, Pan ZF, Liang MZ, *et al.* Highly transparent and color-adjustable Eu^{2+} doped $SrO–SiO_2–Al_2O_3$ multilayered glass ceramic prepared by controlling crystallization from glass. *J Eur Ceram Soc* 2019, **39**: 3856–3866.
[25] Ma YL, Li XC, Wu L, *et al.* Preparation of $(Lu,Y)_3(Al,Sc,Cr)_2Al_3O_{12}$ phosphor ceramics with high thermal stability for near-infrared LED/LD. *J Adv Ceram* 2024, **13**: 354–363.
[26] Yang Z, Liu YF, Yang XY, *et al.* Large-sized $Y_3Al_5O_{12}:Ce^{3+}/Al_2O_3$ composited ceramics for laser-driven lighting sources. *J Am Ceram Soc* 2026, **109**: 70592.
[27] Liu X, Chen MX, Zhao JZ, *et al.* Unique composite architecture of phosphor-in-glass film coated on different heat-conducting substrates for high-brightness laser lighting. *J Adv Ceram* 2025, **14**: 9221027.
[28] Yu ZK, Li JY, Zhao JZ, *et al.* High luminescence saturation $Y_3Al_5O_{12}:Ce^{3+}$-diamond composite color converter for high-brightness laser-driven white lighting. *Laser Photonics Rev* 2025, **19**: 2401124.
[29] Wang GJ, Zhu QQ, Nie SJ, *et al.* Innovative architecture for phosphor-in-glass films enabling superior luminance and color quality laser-driven white light. *Laser Photonics Rev* 2024, **18**: 2301263.
[30] Bendary AA, Gomaa HM, Moneep AM, *et al.* Effect of replacing B_2O_3 with Dy_2O_3 on the structural, physical, and radiation shielding properties of sodium boroaluminate glass. *J Aust Ceram Soc* 2024, **60**: 455–469.
[31] Yu ZK, Zhao JZ, Yang ZZ, *et al.* A novel PiGF@diamond color converter with a record thermal conductivity for laser-driven projection display. *Adv Mater* 2024, **36**: 2406147.
[32] Mhareb MHA, Alqahtani M, Alshahri F, *et al.* The impact of barium oxide on physical, structural, optical, and shielding features of sodium zinc borate glass. *J Non-Cryst Solids* 2020, **541**: 120090.
[33] Zhang HJ, Zhao JZ, Yu ZK, *et al.* A novel sapphire@PiGF@sapphire color converter with high luminescence saturation threshold for laser lighting. *Adv Funct Mater* 2025, **35**: 2414023.
[34] Zhang HJ, Zhao JZ, Yu ZK, *et al.* Omnidirectionally encapsulated phosphor-in-glass film converter for laser-driven lighting source. *Laser Photonics Rev* 2026: 03165.
[35] Hu DH, Lin SS, Pang T, *et al.* Ultra-narrowband green-emitting transparent composite ceramics for laser-driven display. *Adv Mater* 2025, **37**: 2414957.
[36] Guo YQ, Wang GJ, Qiu LR, *et al.* Achieving ultra-brightness green light source with electro-optical conversion efficiency up to 26.3% for underwater wireless optical communication. *Adv Funct Mater* 2025, **35**: 2506929.
[37] Kuang YH, Sun YS, Chen WB, *et al.* Integrating high efficiency and thermal reliability photoluminescence in double-sapphire-sandwiched phosphor-in-glass film for laser projection displays. *Adv Funct Mater* 2026, **36**: 20133.
[38] Zheng P, Li SX, Wei R, *et al.* Unique design strategy for laser-driven color converters enabling superhigh-luminance and high-directionality white light. *Laser Photonics Rev* 2019, **13**: 1900147.
[39] Zheng P, Li SX, Wang L, *et al.* Unique color converter architecture enabling phosphor-in-glass (PiG) films suitable for high-power and high-luminance laser-driven white lighting. *ACS Appl Mater Inter* 2018, **10**: 14930–14940.
[40] Wu HJ, Wu H, Pan GH, *et al.* Cyan–green-emitting $Ca_3Sc_2Si_3O_{12}:Ce^{3+}$ transparent ceramics: A promising color converter for high-brightness laser lighting. *J Adv Ceram* 2023, **12**: 1731–1741.
[41] Deng TL, Huang LH, Li SX, *et al.* Thermally robust orange–red-emitting color converters for laser-driven warm white light with high overall optical properties. *Laser Photonics Rev* 2022, **16**: 2100722.
[42] Zhou TY, Hou C, Zhang L, *et al.* Efficient spectral regulation in Ce:$Lu_3(Al,Cr)_5O_{12}$ and Ce:$Lu_3(Al,Cr)_5O_{12}$/Ce:$Y_3Al_5O_{12}$ transparent ceramics with high color rendering index for high-power white LEDs /LDs. *J Adv Ceram* 2021, **10**: 1107–1118.
[43] Zhang YL, Hu S, Wang ZJ, *et al.* Pore-existing $Lu_3Al_5O_{12}$:Ce ceramic phosphor: An efficient green color converter for laser light source. *J Lumin* 2018, **197**: 331–334.
[44] Hua H, Feng SW, Ouyang ZY, *et al.* YAGG:Ce transparent ceramics with high luminous efficiency for solid-state lighting application. *J Adv Ceram* 2019, **8**: 389–398.
[45] Li SX, Zhu QQ, Tang DM, *et al.* Al_2O_3–YAG:Ce composite phosphor ceramic: A thermally robust and efficient color converter for solid state laser lighting. *J Mater Chem C* 2016, **4**: 8648–8654.
[46] Liu GC, Xiong Z, Chen WB, *et al.* $MgAl_2O_4:Cr^{3+}$ translucent ceramics with tunable broadband near-infrared luminescence for laser-driven light source detection. *InfoMat* 2025, **7**: 70020.
[47] Park J, Kim J, Kwon H. Phosphor–aluminum composite for energy recycling with high-power white lighting. *Adv Opt Mater* 2017, **5**: 1700347.
[48] Wang HT, Kong SY, Tian TF, *et al.* A novel PiGF@coated sapphire color converter with dual optical functions for high-brightness laser-driven projection display. *J Lumin* 2025, **287**: 121467.
[49] Peng Y, Yu ZK, Zhao JZ, *et al.* Unique sandwich design of high-efficiency heat-conducting phosphor-in-glass film for high-quality laser-driven white lighting. *J Adv Ceram* 2022, **11**: 1889–1900.
[50] Yu ZK, Chen MX, Zhao JZ, *et al.* A universal PiGF@sapphire@MiG color converter with synergistically enhanced opto-thermal performance for laser-driven applications. *Adv Opt Mater* 2026, **14**: 01953.
[51] Mou Y, Chen DY, Tian B, *et al.* High-quality laser-driven white lighting enabling by collecting backward emission light of phosphor-in-glass film. *IEEE T Electron Dev* 2024, **71**: 1139–1144.
[52] Zhao JZ, Mou Y, Yu ZK, *et al.* Microstructured interface modification of laser-driven phosphor-in-glass-film for ultra-high-efficiency white lighting. *J Alloy Compd* 2023, **960**: 170744.
[53] Ding WT, Yang S, Hou X, *et al.* High performance composite phosphor-in-glass film for laser-driven warm white light on patterned sapphire substrate. *J Materiomics* 2025, **11**: 100892.
[54] Chen WB, Wang YZ, Xu J, *et al.* Red-emitting cordierite ceramic enabling general healthy warm white laser lighting. *Laser Photonics Rev* 2024, **18**: 2300963.